□□□□

□□□ CO_2--□□□□□ CO_2 □□ □□□ □□□□□□□□□□□□□□□□ 1)

□ □ *,† □□□ *,2) □□□ † □□□ *

*(□□□□□□□□□□□□□□□□□□□□□□□□□□□□□ 430072)

†(□□□□□□□□□□□□□□□□□□□□□□□□□□□□□ 94720)

□□ CO_2 □□□□□□□□ CO_2 □□□□□□□□□□□□□□□□□ □□□□□□□□□ (□□□) □□□ CO_2 □□□□□□□□□□. □ □□□□□-- □□□-- □□□□□□□□□□□□□□□□ CO_2 □□ (8.5 MPa, 45°C) □ CO_2 □□□ (□□) □□□□ CO_2(□□) □□□□□□□□□□□□□□□□ CO_2 □□□□□□□□ □□□□□□□□□□□□□□□□□□□□□□□ CO_2 □□□□□□. □ □□□□□□□□□□□□□□□□□□□□□□□□□□□□□□□□. □□□□ □□ □□□□□ CO_2 □□/□□□□□□□□□□□. □□□□□□□□□□ □□□ CO_2 □□□□□□□□□□□□□□□□□□□□□□□□□□□□□□□□ □□□□

3 □□□□□□□□□□□□ (□ Jurauld □□□Land □□□ Spiteri □□) □□□. □□□□□Jurauld □□□□□□□□□□ □ Land □□□Spiteri □□□□□□□□□□. □□ Land □□ □□ □□□□ Land □□.

□□□ CO_2 □□□□, □□□□, □□□, □□□□, □□□□

□□□□□□O363.2, V211.1+7 □□□□□□A

doi□ 10.6052/0459-1879-16-237

□□□□□□□, □□□, □□□, □□□. □□□ CO_2--□□□□□ CO_2 □□□□□□□□□□□□□□□□□□□□□□□□. □□□□, 2017, 49(3): 638-648

Hu Ran, Chen Yifeng, Wan Jiamin, Zhou Chuangbing. Supercritical CO_2 water displacements and CO_2 capillary trapping: micromodel experiment and numerical simulation. *Chinese Journal of Theoretical and Applied Mechanics*, 2017, 49(3): 638-648

SUPERCRITICAL CO_2 WATER DISPLACEMENTS AND CO_2 CAPILLARY TRAPPING: MICROMODEL EXPERIMENT AND NUMERICAL SIMULATION 1)

Hu Ran*,† Chen Yifeng*,2) Wan Jiamin† Zhou Chuangbing*

*(*State Key Laboratory of Water Resources and Hydropower Engineering Science*□*Wuhan University*□*Wuhan* 430072□*China*)

†(*Lawrence Berkeley National Laboratory*□*Energy Geosciences Division*□*Berkeley CA* 94720□*USA*)

Abstract The CO_2 capillary trapping is an important scientific issue in geological carbon sequestration, but few re- searches focus on the trapping mechanism at pore scale under supercritical CO_2 condition. In this study, based on the high-pressure fluids-microscopy-micromodel experimental system, we performed drainage experiment, i.e. supercrit- ical CO_2 displacing water, and imbibition experiment, i.e. water displacing CO_2, under the conditions of 45°C and 8.5 MPa. The DSLR camera was used to capture pictures of CO_2-water two-phase immiscible flow and the microscopy was used to capture the capillary trapping behavior for the supercritical CO_2 at the pore scale. The computational fluid dynamic method was adopted to simulate the two-phase fluid flow processes. The numerical results are generally in agree- spacement with the experimental observations, and further provide three-dimensional geometries on the interface during the drainage-imbibition processes and the trapped supercritical CO_2 droplet/cluster. Finally, the capillary trapping curve, i.e. the relationship between the initial CO_2 saturation and the residual saturation, was obtained from the numerical results, and we made an assessment of the three capillary trapping models, i.e. Land's, Jurauld's and Spiteri's trapping models. A comparison of the models performance indicates that Jurauld's model behaves slightly better than Land's model, whereas Spiteri's model behaves poorly. However, given that Land's model only contains one parameter of clear physical meaning, it is recommended for practical use.

2016–08–26 □□□2017–02–14 □□, 2017–02–15 □□□□□.

1) □□□□□□□□(51409198, 51579188) □□□□□□□□□□(2015T80833) □□□□.

2) □□□, □□, □□□□□□□□□□□□□□□□□□□□□□□□□. E-mail□ csyfchen@whu.edu.cn

Key words geological carbon sequestration, micromodel, two-phase flow, numerical simulation, capillary trapping

□□□□□□□□□□□□□□□□□□ CO_2 □□□□□□□□□□□□□□□□ □□. □□□CO_2 □□□□ (geological carbon sequestration, GCS) □□□□□□□□ CO_2 □□□□□□□□□□□□□□□□. □□□□ CO_2 □□□□□□□□□□□□□□□□□□□□□□□□.

CO_2 [1]. [2] CO_2 2005 — 2050 20%~50%. CO_2 [3-4]. CO_2 800 m CO_2 CO_2 CO_2 CO_2 . (capillary trapping residual trapping)[5]. GCS CO_2 [6] CO_2 CO_2 CO_2 .

space [18-20]. Al-Raoush[8] . Chaudhary [10] CO_2 CO_2 . Andrew [21] CO_2 CO_2 . [22] CO_2 (sc CO_2) CO_2 . Niu [17] CO_2 CT CO_2 .

CT [23-25]. [18-20] [26] [27] . Lenormand [20] Zhang [28]

space

CO_2

space CO_2 (CT) [7-10]

space . Cottin [29]

space [10-12] CO_2 [13-14] . CO_2 . CO_2 . (1) CT(computed tomography) [15-17]; (2) /

space . CO_2 CO_2 .

[30] [31] [32] [33-34]. 3 [35]. .

-- -- CO_2 (8.5 MPa45°C) CO_2 CO_2 -- . CO_2 (3).

1

1.1 --

1(a) CO_2 CO_2 .

(1) (Carl Zeiss, AxioCam MRc5) (Carl Zeiss, Observer Z1.m) . 20 mm 10 mm 50 μm 40 μm (pore volume) 1.97 μL 1(b). . (20 mm × 10 mm) (1 /) ( ) .

(2) (Tele- dyne ISCO, 500HP×2 65 HP) . 1(a) A CO_2 B C (8.5 MPa).

(3) CO_2 (Parr, model 4560) A CO_2 . CO_2 (1.97 μL) CO_2 (H_2CO_3) CO_2 [24]. A (8.5 MPa)

space CO_2 .

(4) . (1)(2) (3) (Omega, Type T) (Cole Parmer, EW-89000-10) (45±1)°C.

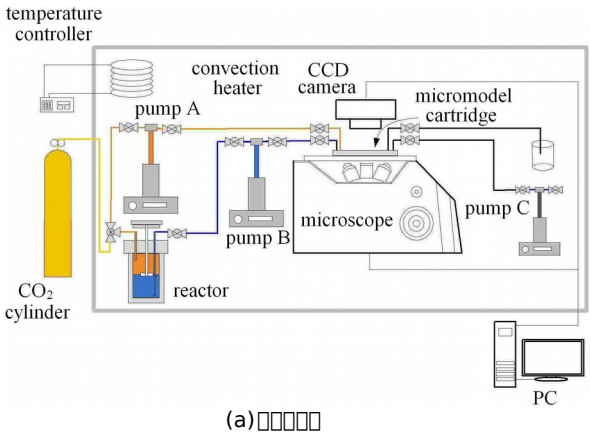

(a)

(a) Experimental apparatus

(b) □□□□□□

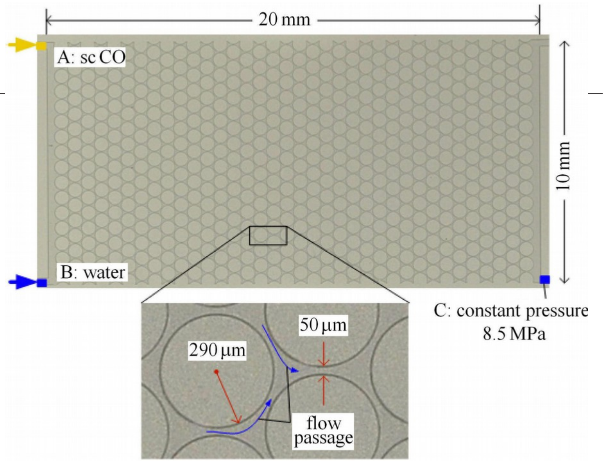

(b) The sizes of the micromodel

图 1 □□□□--□□□--□□□□□□□□

Fig. 1 High-pressure fluids-microscopy-micromodel system

1.2 □□□□

□□□□□□ CO_2□□□□□□□□□□□□□□□□□□□CO_2 □□□□□CO_2 □□□□□□□ 4 □□□. □□□□ 3 □□□□□□□□□

(1) CO_2 □□□□□□□□. □□□□□□□□□ CO_2 □□□□□□□□□□□□□□□ CO_2 □□□□

space □□□□□□. □□□□□□□□□□□□□□□□□□□□□ NaCl(Sigma-Aldrich, ACS reagent grade) □□ 0.01 mol/L □ NaCl □□. □□□□□□□□□□□□□ CO_2 □□□□□□ A. □ A □□□□□□□□□□□□□□□□□□□□ 8.5 MPa □ 45°C. □□□□□□□ 24 h□□□ CO_2 □□□□□□□□.

(2) □□□□□□. □□□□□□□ 500 μL/min □□□□□□□□□□□ 10 min□□□□□□□□□□□ 120°C □□□□ 24 h.

(3) CO_2 □□□□. □□□□□□□ C □□□□□□□□□□□□□□□□□□□□□□□□□□□ □□□□□□ 8.5 MPa. □□□ C □□□□□□□□□ □□□□□□ (0.01 mol/L NaCl) □ 200 μL/min □□

space □□□□□. $\boldsymbol{f}_s$ □□□□

$$\boldsymbol{f}_s = \sigma \cdot \kappa \cdot \boldsymbol{n} \cdot \delta_{\Gamma_T} \tag{3}$$

□□, σ □□□□□, κ □□□, $\boldsymbol{n}$ □□□□□□□□ (□□) □□□□□□□δ_{Γ_T} □ Dirac delta □□□□□□□ 1□□□□□ 0.

□ (1) □□□□□□□□□□□□□□□□ (1) □□□□□□□□□□□□. □□□□□□□□□□□□□□□□□□□□□ (volume of fluid□VOF) □□□□□□□ [35]. □□□□□□□□□□□□□□□□□ α□□□□□□□□□□□□□□ (□□ 2 □□)

$$\alpha = \begin{cases} 0, & \text{in the nonwetting phasec } (CO_2) \\ 1, & \text{in the wetting phase } (CO_2) \\ 0 < \alpha < 1, & \text{on the interface} \end{cases}$$

space □□□□□□□□□ 5 min. □□□□□□ A □□□□□□□CO_2 □□□□□□ A □□□. □□□□□□□ 3 h□□□□ CO_2 □□□□□□□□□. 3 h □□□ A □ 192 μL/min □□□□□□□□□□□□□□ CO_2 □□□□□□□□□□□□□ (drainage). □□□□ 1 □/□□□□□□□□. □□□□□□□□□□□□ (1.97 μL)□□□□□□□□□ 2 s □□□□□□□□. □□□□□□□□ A □□□□□□□□□□ B □□□□□□□□□□□□□□(192 μ L/min) □□□□□□□□□ (imbibition). □□□□□□ 3 s □□□□□□□□

(4) CO_2 □□□□□□□. □□□□□□□□□□□□□□□□□□□□□□□□. □□□□□□□□□□□5 min □□□□□□□□□□□□□□□□. □

space(4)

space □□□□□□□□□□□□□□□□□□□□□ CO_2 □□/□□□□□□□□.

□□□□□□□□□□ [23] □□□□□□□□□□□□□□□□□ [23].

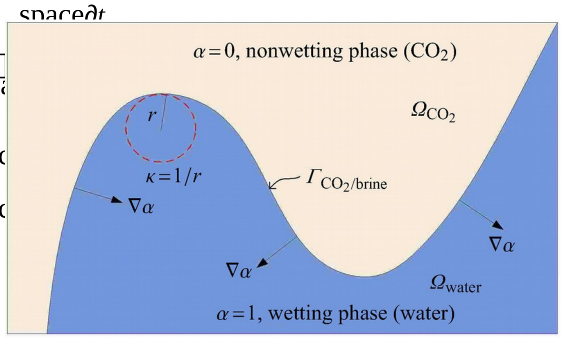

图 2 □□□□□□□□

Fig. 2 Illustration of the volume of fluid method

2 □□□□

2.1 □□□□

□□□□□CO_2 □□□□□□□□□□□□

space □□□□□□□□□□□□□□□□□□□□□□□□□□

$$\frac{\partial\alpha}{\partial} + \nabla \cdot (\alpha \boldsymbol{u}) + \nabla \cdot [\alpha \cdot (1-\alpha)\boldsymbol{u}_r] = 0 \tag{5}$$

□□□$\boldsymbol{u}_r$ □□□□□□□□□□□□□□□□□□□□□□□□□□[36].

□□□ (4)□□ (1) □□□□□□□□□□□□□□□□□□□□□□

space □□--□□□□□□□□□□□□□□□□□□□

$$\frac{\partial(\rho\boldsymbol{u})}{\partial t} + \nabla \cdot (\rho\boldsymbol{u}\boldsymbol{u}) = -\nabla p + \nabla \cdot \left[\mu\left(\nabla\boldsymbol{u} + \nabla^T\boldsymbol{u}\right)\right] + \boldsymbol{f} \tag{1}$$

$$\mu = \alpha\mu_w + (1-\alpha)\mu_{CO_2} \tag{6}$$

□□ ... ρ_w +

σπ αχ ε□ □□ μ_w □

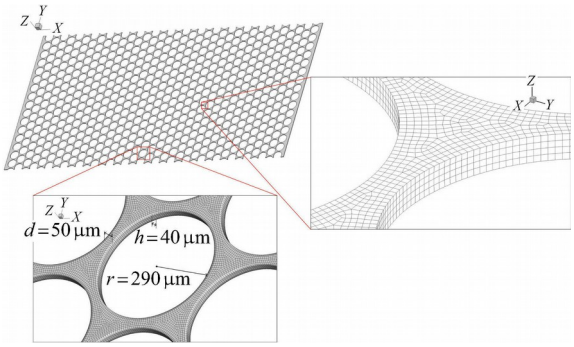

$$\nabla \cdot \boldsymbol{u} = 0 \tag{2}$$

ρ_{CO_2}

CO_2

.

$\boldsymbol{u}$, p μ $\boldsymbol{f}_s$ CO_2

$\boldsymbol{n} = \nabla\alpha$ $\kappa = \nabla \cdot (\nabla\alpha/|\nabla\alpha|)$. $\boldsymbol{n}$, κ α (3) (1)

(2) (5) CO_2 [35]

$\nabla\alpha$ 1

: $\boldsymbol{n}$ cos

$\boldsymbol{n}$ sin

(8)

$\mu(\alpha)$ $\nabla\boldsymbol{u} + \nabla^T\boldsymbol{u}$

$+ \nabla \cdot (\rho(\alpha)\boldsymbol{u}\boldsymbol{u})$ +

$\nabla \cdot \boldsymbol{u}$

$\nabla p + \sigma \cdot \nabla \cdot$

$= 0$

$\nabla\alpha$

$\nabla\alpha$

$\cdot \nabla\alpha \cdot \delta_\Gamma = 0$

θ $\boldsymbol{n}_s$ $\boldsymbol{n}_t$

.

$\boldsymbol{u} = 0$ $\alpha = 1$ $p = 8.5$ MPa.

$$\sigma\pi\alpha\chi\varepsilon\frac{\partial\alpha}{} + \nabla \cdot (\alpha\boldsymbol{u}) + \nabla \cdot [\alpha \cdot (1-\alpha)\boldsymbol{u}_r] = 0$$

μ_{CO_2}

CO_2

μ_w

2.2

space (7)

space(1) (drainage) A $u = 0.32$ m/s ($\nabla p = 0$ $\alpha = 0$ $\partial u/\partial x = \partial u/\partial y = \partial u/\partial z = 0$ $p = 8.5$ MPa $\nabla\alpha = 0$(2) OpenFOAM[36]

. Open-FOAM (7) . 3 1 962 924 2 712 905 6~9 μm. 1 .

3

Fig. 3 Finite volume mesh for the micromodel

1 CO_2

Table 1 The parameters for the supercritical CO_2-water two-phase fluid flow

(imbibition) B $u = 0.32$ m/s ($\nabla p = 0$ $\alpha = 1$ $\partial u/\partial x = \partial u/\partial y = \partial u/\partial z = 0$ $p = 8.5$ MPa $\nabla\alpha = 0$(3) (B $u = 0$ m/s $p = 8.5$ MPa $\nabla\alpha = 0$.

. II

96 CPU CO_2 23 040 ·. 3.3 768 CPU 115 200 ·.

3

1.2 3 3 .

CO_2 CO_2 /1 CO_2 3 . I $\nabla\alpha$ [39] CO_2 .

3.1 CO_2

4 θ

space45°C, 8.5 MPa

spaceWater (NaCl 0.01 mol/L)

spaceSupercritical CO_2

3 .

3 (*Ca*)

density/(kg·m^{-3})	993.9[37]	281.8[a]
viscosity/(kg·s^{-1}·m^{-1})	5.972×10^{-4}[a]	$2.275\ 8\times10^{-5}$[a]
interfacial tension /(N·m^{-1})	33.1 ± 0.5[38]	

(*M*). *Ca* *M*

u

Note: a from National Institute of Standards and Technology (NIST) web-based database (http://webbook.nist.gov/chemistry/fluid/)

$$Ca = \frac{\mu_i}{\sigma}$$

$$M = \frac{\mu_i}{\mu_2}$$

(9)

(10)

. 8.5 MPa 45°C 10 CO_2 22°. OpenFOAM

space □□, u_i □ μ_i □□□□□□□□□□□□□□□□□□ □□μ_2 □□□□□□□□□□□□. □□□□□□□□□□□Lenormand □ (□□)[20] □ Zhang □ (□□)[28] □□□□□□□□□□□□□□□ 4 □□.

space

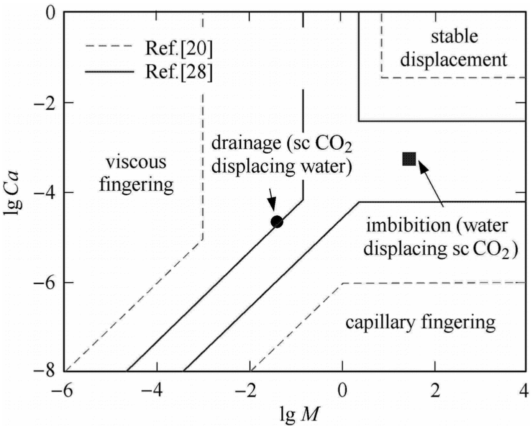

□ 4 □□□□□□□□□□□□□□□

Fig. 4 The phase diagram for displacement pattern within the two-phase immiscible fluid flow

□□ 1 □□□□□□□ (8) □□ (9) □□□□□□□□□ (drainage□CO_2 □□□)□□□□□□□□□□□□□$Ca = 2.24 \times 10^{-5}$□$M = 0.038$□□□□□□ (im-bibition□□□□ CO_2)□$Ca = 5.87 \times 10^{-4}$□$M = 26.24$. □□ 4 □□□□□□□□□□□□ (drainage)□□□□□□□□□□□□□□□□□□□□□.

□ 5 □□□□□ 0.1 s □□□□□□ CO_2 □□□□□□□□□. □ □ CO_2 □□□□□□□□□ □□□□□□□□□□□□□□□ CO_2 □□□□ □□□□. □□□□□CO_2 □□□□□□□□□□□□□□□. □□□□□□□□□ □□□□□□□□□□□□□CO_2 □□□□□□□□□□□□□□□CO_2 □ □□□□□□□□. □ 5 □□□□□□□□□□□ CO_2 □□□□□□CO_2 □□□□□□□□□□. □□□□□□□□□□□□□□□ □□□□□□□□ (□□) □□.

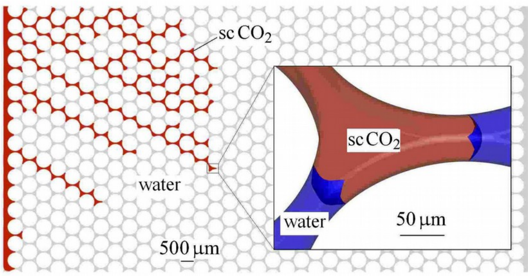

space □ 6 □□□□□ 1 s □□CO_2 □□□□□□□□□□□□□ □□□□. □□□□□□□ 1 s □□□ □□□ (CO_2) □□□□□□□ □□□. □□□□□□□□□□□□□□□□□□□□□□□□□□□□□□□□CO_2 □□□□□□□□. □ 6(a) □ CO_2 □□□□ 51.1%□□ □□□□ CO_2 □□□□□□□ (51.0±3.9)%. CO_2 □□□□□□□ □□□□ 53.9%(□ 6(b)). □□□□□□CO_2 □□□□□□□□□ □(58.3±2.1)%□□□□□□□□ 61.3%□□□□□□□.

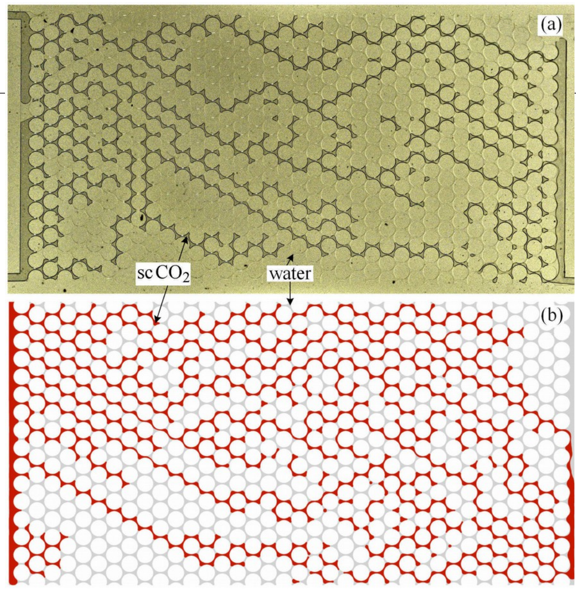

Fig. 6 Comparison between numerical results and the DSLR captured images after 1 s of drainage ((a) experimental result, (b) numerical simulation)

□ 6 □□□□(drainage)1 s □□□□ (□□□□□□) □□□□□□□((a) □□□□, (b) □ □□□□□)

□□□□□□ 2 s □□□□□□□□□□□□□□□□□□□□□□□□□□□□□□□□□ CO_2. □ 7 □□□□□ 0.1 s □□CO_2 □□□□□□□□□□□. □□□□□□□□□□□□□□□CO_2 □□□□□□□□□□□□□□□□□□□ “□□□” □□□ CO_2. □ 7 □□□□□□□□□□□□□□□□□□□□ CO_2 □□□□□□□□□□□□.

□□ 1 s □□CO_2 □□□□□□□□□□□□□□□□□□ 8 □□. □□□□□□□ 1 s □□□□□□□□□□□□ CO_2 □□□/□□□□□□□□□

space □ 5 □□□□ (drainage)0.1 s □□□□□□□□

space □□□□□□. CO_2

space □□□□□□□□□□□□□□

spaceFig. 5 The numerical results for the two-phase fluid flow after 0.1 s of drainage

space □□□□□□□□□□□□□□□. □□□□□□, □

space

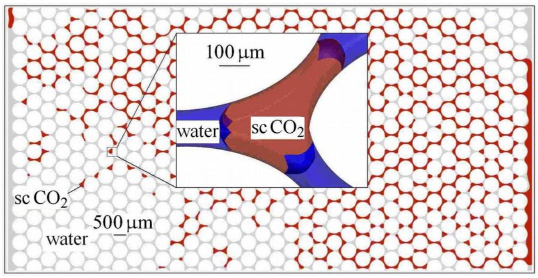

□ 7 □□□□(imbibition) 0.1 s □□□□□□□□

Fig. 7 The numerical results for the two-phase fluid flow after 0.1 s of imbibition

□□□□□□ (□□□□□□□□□□)□□□ “□□□” □□ CO_2□□□ CO_2 □□□□□□□□□. □□□□□□□□□□□ CO_2 □□□□□. □□□□□□□□(drainage)□□□□□□□□□□□ CO_2 □□□□□□□□ (□ 8(a)). □□□□□□ (imbibition)□□□□□□□□□□□□□□ CO_2 □□□□□□□□□□□□□□□□□□□□□□□□□□□□□ CO_2 □□□□□. □□□□□□□□□□□□□□□□□□□ □□□ CO_2 □□□□□□□□.

□ 8(a) □ CO_2 □□□□ 29.4%□□□□□□

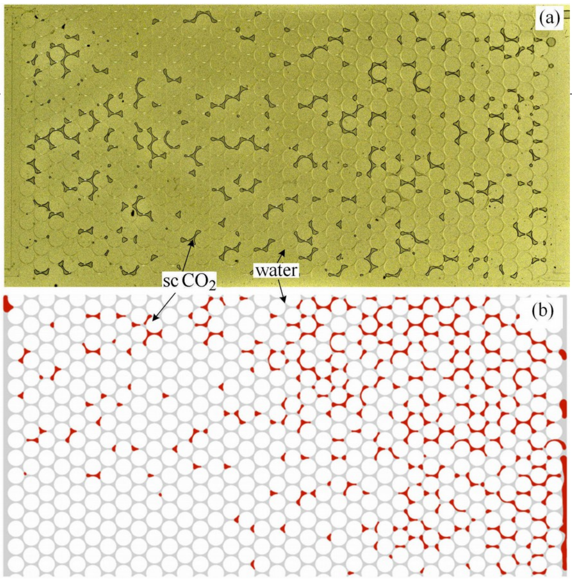

□ 8 □□□□(imbibition) 1 s □□□□(□□□□□□) □□□□□□□□ ((a) □□□□, (b) □□□□□□)

Fig. 8 Comparison between numerical results and the DSLR captured images after 1 s of imbibition ((a) experimental result, (b) numerical simulation)

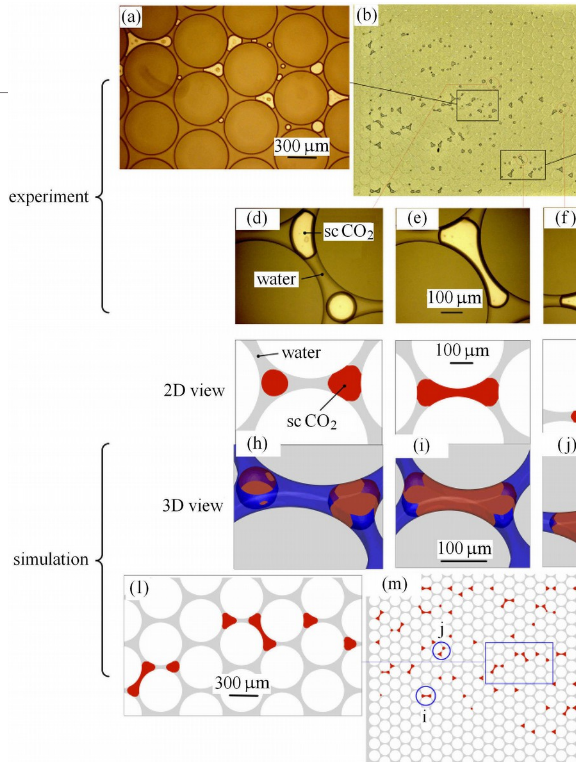

□ 9 □□□ CO_2 □□□□□□□□(a) ~ (g) □□□□□□□(h) ~ (n). (a) □(c) □□□□□□□□□□□□□ CO_2 □□/□□□□□(b) □□□□□□□□□□ CO_2 □□/□□□□□□□ (d) ~ (g) □□□□□□□□□□□□□□□□□□□ CO_2 □□□□□□. (m) □□□□□□ CO_2 □□/□□□□□□□(l) □ (n) □□□□□ CO_2 □□□□□□□□□□□□□(h) ~ (k) □□□□□ CO_2 □□□□□□□□□□□□ Fig. 9 The observed (a) ~ (g) and simulated (h) ~ (n) shape and distribution of trapped CO_2 droplets/clusters: (a) and (c) the distribution of trapped CO_2 droplets/clusters at multiple pores; (b) the distribution of trapped CO_2 droplets/clusters at the full scale of micromodel; (d) ~ (g) the distribution of trapped CO_2 droplets/clusters at a single pore. (m) the distribution of trapped CO_2 droplet/cluster at the full scale of micromodel; (l) and (n) the distribution of trapped CO_2 droplets/clusters at multiple pores; (h) ~ (k) the distribution of trapped CO_2 droplets/clusters at a single pore

space □□□□□□□ (27.7±2.3)%□□□□□□□□ 21.9% (□ 8(b)). □□□□□□□□ 1 s □□□□□□□□□□□□□□□□□□□. □□□□□□□□□: (1) □□□□□□□□□□□□□□□□□ CO_2□□□□□□ (im-bibition) □□□□□□□□□□□□□□ CO_2 □□□□□□□□□□(2) □□□□□□□□□□□□□□□□□ (□ 0.5 μm) □□□ (□□□)□□□□□□□□□□□□□□□□□□□□. □□□□□□□□□□□□ 50 μm□□□□ 40 μm□□□□□□□□□□□□□□□□□□□□□□□□□□. □□□□□□□□□□□□□□□□□□□□□□□□□□□□□□□□□□□□□□(3) □□□□□□□□□□□□□□□□□□□□□□□□□□□□. □□□□□□ 10^{-4} □□[40–41].

3.2 CO_2 □□□□□□□□□□□□□□□□□

□□□ CO_2 □□ 3 s □□□□□□□□. □□□□□□□□□□□□□. □□ (8.5 MPa). □□□□□□□□□□□□□□□□□□□□□□ 5 min □□ □□□□□□□□□. □ 9 □□□□□□□□□□□□ CO_2 □□/□□□□□□□. □□□□□□□□□□□□□□□□□□□□□□□□ CO_2 □□□□□□□□□□□□□□□□□CO_2 □□□□□□□□ (□□□□□)□□□□□□□□□□□□□□□□□□□□□ [8,10]. □□□□□□□□□□□□□□□(pore body) □ (□ 9(d), □ 9(f) □□ 9(g))□□□□□□□□□□□□□ (□ 9(e))□□□□□□□□□□□□. □□□□□□□□□□□□□□□□ CO_2 □□/□□□□□□□□□. CO_2 □□□□□□□□□□□□□ 9(h) ~ □ 9(n) □□. □□□□ CO_2 □□/□□□□□□□□□□□(□ 9(h)□□ 9 (j) □□ 9 (k))□□□□□□□□□□□□□□ (□ 9(i)). □□ 9(h) ~ □ 9 (k) □□□□□□□□□□□□□□□□CO_2 □□□□□□□□□□□□□□□ CT □□□□□□□□□□□□[8].

□□ 9(b) □□□CO_2 □□□□□□ 10.3%□ □□□□□□□□□ (9.2±1.1)%□□□□□□□□ 7.9%(□ 9(m)). □□ CO_2 □□□□□□□□□□□(□□□□) □□□□□□□□ [42–43]□□□□□□□ 1×10^{-6} □□□□□□ $S_{nwr} \sim \lambda \lg(Ca)$ □□□□□ λ space □□□. □□□□□□□□□□□□□□□□□□□□□□□□□□□□□□□□□□. □□□□□□□□□ (imbibi- tion)□□□□□ $Ca = 5.87 \times 10^{-4}$□$M > 1$□□□□□□□□□□□□□□□□□□□□□□□□□□□□□□□□□□□□□ (□ 4).

□□□□□□□□□□□□□□□□□□□□□ □□□□□□□□□ 192 μL/min□□□□□□□□□□□□□□□. □□□□□□□□□□□□□□ 10 MPa □□□□□□. □□□□□□□□□□□□□□□□ [24,44]□□□□□□□□□□□□□□□□□. □□□□□□□□□□□□□□□ (□□□□□□) □□□□□□□□□□□□□□□□□□□□. □□□□ space □□□□□□□□□□□□□□□□□□□□□□ □□□□□□□□□□□□□□□□□□□□□□□□□□□□□□□□□□□□□. □□□□□□□□□□□□□□□□□□□□□□ □□□□□□□□□□□□□□□□□□□□□□□□□ □.

3.3 □□□□□□□□/□□□□□□□□□□□□

□ CO_2 □□□□□□□□□□□□□□□□□□□□□□□□□ (S_{nwi}) □□□□□□ (S_{nwr}) □□□□□□□□□□□□□□□□□□□□□□□□. Land[45] □□□□□□□□□□□□□□□□□□□□□. Land □□□□□ space □□□□□□□□□□□□□□□□□□□□□□ □□□□□□□□□□□□□□□□ [23]. □□□□□

space S_{nwr}

space

$$= \frac{S_{nwi}}{1 + C S_{nwi}} \qquad (11)$$

□□□□□□□□□□□□□□ 8.5 MPa □□□□□□□□□□□□□□□□ (6 h)□□□□□□□□□ "□□" □□□. □□□□□□□□□□□□□□□□ □□, S_{nwi} □ S_{nwr} □□□□□□□□□□□□□□□□ C □ Land □□□□. S_{nwi} □□□□□□□□□□□□□□□□□□□□□□□□□□□□□□. Land □□□□□

□□□□□□□□□□□□□□□□□□□□□□□□

$$C = \frac{1}{S_{nwr,max}} - \frac{1}{S_{nw,max}} \qquad (12)$$

□□, $S_{nwr,max}$ □ $S_{nw,max}$ □□□□□□□□□□□□□□□□□□□□□□. Jerauld[46] □ Land □□□□□□□

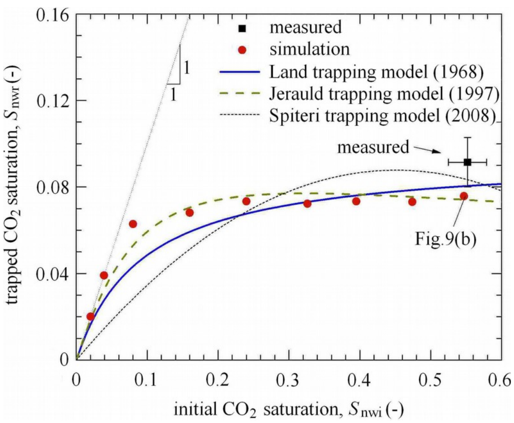

[illegible]

$$S_{nwr} = \frac{S_{nwi}}{1 + C S_{nwi}^{1+b/C}} \quad (13)$$

[illegible], b [illegible]. [illegible] (11) [illegible] (13) [illegible] $b = 0$ [illegible]Jerauld [illegible]Land [illegible].

Spiteri [illegible] [47] [illegible]

[illegible] 10 [illegible] CO_2 [illegible] Fig. 10 The comparison of the capillary trapping curve between the numerical simulation/experimental data and three different models

[illegible] 10 [illegible] 7% [illegible]

$$S_{nwr} = \alpha S_{nwi} - \beta S_{nwi}^2 \quad (14)$$

[illegible], α [illegible] β [illegible].

[illegible] 1:1 [illegible] CO_2 [illegible] 0.07 [illegible] CO_2 [illegible]. [illegible]Jerauld [illegible] Land [illegible]

[illegible] 3 [illegible]. [illegible] CO_2 [illegible] CO_2 [illegible]. [illegible] 5 s [illegible]. [illegible] S_{nwi} [illegible] S_{nwr} [illegible] ([illegible] 2 s) [illegible].

[illegible] 10 [illegible]. [illegible] 2 [illegible]. [illegible] 2 [illegible]Jerauld [illegible] Land [illegible] 0.006 6 [illegible] 0.01[illegible] Spiteri [illegible] 0.019 0. [illegible]Jerauld [illegible] Land [illegible] Jerauld [illegible] Land [illegible]Spiteri [illegible].

[illegible] 2 [illegible]

Table 2 The fitting parameters and the root-mean-square-error (RMSE) for the three models

Prediction model	Optimal fitting coefficient	Mean-squared error
Land mode, Eq.[10]	C = 10.62	0.010 0
Jerauld mode[illegible]Eq.[12]	C = 14.09, b = 4.42	0.006 6
Spiteri mode[illegible]Eq.[13]	α = 0.389 4, β = 0.431 8	0.019 0

Spiteri [illegible]. [illegible] 30% [illegible]. Jerauld [illegible] Land [illegible] Spiteri [illegible] 45% [illegible]. [illegible] 10 [illegible]. [illegible] S_{nwi} = (58.3 ± 2.1)%[illegible]S_{nwr} = (9.2 ± 1.1)%[illegible]S_{nwi} = 61.3%[illegible]S_{nwr} = 7.9%[illegible]. [illegible] 3.1 [illegible] 3 [illegible]. Raeini [illegible] [33] [illegible] LV60 [illegible] CO_2 [illegible] 0.5 [illegible]CO_2 [illegible] 2%~4%. [illegible] 1.3%.

4 [illegible]

[illegible] -- [illegible] -- [illegible] CO_2 [illegible] CO_2 [illegible] CO_2 [illegible] OpenFOAM [illegible] CO_2 [illegible] 3 [illegible].

(1) [illegible] CO_2 [illegible].

(2) [illegible] CO_2 [illegible]/[illegible]. [illegible] CO_2 [illegible]/[illegible].

(3) [illegible] 3 [illegible]. [illegible] Jerauld [illegible] Land [illegible] Land [illegible]. [illegible] Land [illegible].

[illegible] CO_2 [illegible]. [illegible] CO_2 [illegible] CO_2 [illegible]. [illegible] GCS [illegible] CO_2 [illegible].

1 Zhang W, Li Y, Xu T, et al. Long-term variations of CO_2 trapped in different mechanisms in deep saline formations: a case study of the Songliao Basin, China. *International Journal of Greenhouse Gas Control*, 2009, 3(2): 161-180
2 Metz B, Davidson O, De Coninck H, et al. IPCC special report on carbon dioxide capture and storage. Prepared by Working Group III of the Intergovernmental Panel on Climate Change. IPCC, Cambridge, United Kingdom and New York, USA: Cambridge University Press, 2005
3 □□□, □□□, □□□. □□□□□□□□□ CO_2 □□□□□ □□□. □□□□□□□□□, 2006, 25(5): 963-968 (Li Xiaochun, Liu Yanfeng, Bai Bing, et al. Ranking and screening of CO_2 Saline aquifer storage zones in China. *Chinese Journal of Rock Mechanics and Engineering*, 2006, 25(5): 963-968 (in Chinese))
4 □□□, □□□, □□□. □□ CO_2 □□□□□□□□□□□□□. □□□□, 2009, 30(9): 2674-2678 (Li Xiaochun, Fang Zhiming, Wei Ning, et al. Discussion on technical roadmap of CO_2 capture and storage in China. *Rock and Soil Mechanics*, 2009, 30(9): 2674-2678 (in Chinese))
5 Suekane T, Nobuso T, Hirai S, et al. Geological storage of carbon dioxide by residual gas and solubility trapping. *International Journal of Greenhouse Gas Control*, 2008, 2(1): 58-64
6 Al Mansoori SK, Itsekiri E, Iglauer S, et al. Measurements of non-wetting phase trapping applied to carbon dioxide storage. *International Journal of Greenhouse Gas Control*, 2010, 4(2): 283-288
7 Tanino Y, Blunt M. Laboratory investigation of capillary trapping under mixed-wet conditions. *Water Resources Research*, 2013, 49(7): 4311-4319
8 Al-Raoush RI. Impact of wettability on pore-scale characteristics of
space
residual nonaqueous phase liquids. *Environmental Science & Tech- nology*, 2009, 43(14): 4796-4801
9 Iglauer S, Pentland C, Busch A. CO_2 wettability of seal and reservoir rocks and the implications for carbon geo-sequestration. *Water Resources Research*, 2015, 51(11): 729-774
10 Chaudhary K, Bayani Cardenas M, Wolfe WW, et al. Pore-scale trapping of supercritical CO_2 and the role of grain wettability and shape. *Geophysical Research Letters*, 2013, 40(15): 3878-3882
11 Tanino Y, Blunt MJ. Capillary trapping in sandstones and carbonates: Dependence on pore structure. *Water Resources Research*, 2012, 48(8): W08525
12 Moura M, Fiorentino EA, Måløy K, et al. Impact of sample geome- try on the measurement of pressure-saturation curves: Experiments and simulations. *Water Resources Research*, 2015, 51(12): 8900- 8926
13 Kimbrel EH, Herring AL, Armstrong RT, et al. Experimental characterization of nonwetting phase trapping and implications for geologic CO_2 sequestration. *International Journal of Greenhouse Gas Control*, 2015, 42: 1-15
14 Chatzis I, Kuntamukkula M, Morrow N. Effect of capillary number on the microstructure of residual oil in strongly water-wet sand- stones. *SPE Reservoir Engineering*, 1988, 3(3): 902-912
15 El-Maghraby RM, Blunt MJ. Residual CO_2 trapping in Indiana limestone. *Environmental Science & Technology*, 2012, 47(1): 227- 233
16 Andrew M, Bijeljic B, Blunt MJ. Pore-scale imaging of trapped su- percritical carbon dioxide in sandstones and carbonates. *Interna- tional Journal of Greenhouse Gas Control*, 2014, 22: 1-14
17 Niu B, Al-Menhali A, Krevor SC. The impact of reservoir conditions on the residual trapping of carbon dioxide in Berea sandstone. *Water Resources Research*, 2015, 51(4): 2009-2029
18 Zhang C, Oostrom M, Grate JW, et al. Liquid CO_2 displacement of water in a dual-permeability pore network micromodel. *Environmental Science & Technology*, 2011, 45(17): 7581-7588
19 Wang Y, Zhang C, Wei N, et al. Experimental study of crossover from capillary to viscous fingering for supercritical CO_2–water displacement in a homogeneous pore network. *Environmental Science & Technology*, 2012, 47(1): 212-218
20 Lenormand R, Touboul E, Zarcone C. Numerical models and experiments on immiscible displacements in porous media. *Journal Of Fluid Mechanics*, 1988, 189: 165-187
21 Andrew M, Bijeljic B, Blunt MJ. Pore-scale imaging of geological carbon dioxide storage under in situ conditions. *Geophysical Research Letters*, 2013, 40(15): 3915-3918
22 □□□, □□, □□□. □□□□□□□ CO_2. □□□□, 2014, 28(5): 1061-1067 (Wu Aibing, Li Yi, Chang Chun, et al. The residual gas saturation of different components of saline flooding CO_2. *Geoscience*, 2014, 28(5): 1061-1067 (in Chinese))
23 Kim Y, Wan J, Kneafsey TJ, et al. Dewetting of silica surfaces upon reactions with supercritical CO_2 and brine: pore-scale studies in micromodels. *Environmental Science & Technology*, 2012, 46(8): 4228-4235
24 Chang C, Zhou Q, Kneafsey TJ, et al. Pore-scale supercritical CO_2 dissolution and mass transfer under imbibition conditions. *Advances*
space
space*in Water Resources*, 2016, 92: 142-158
25 Chang C, Zhou Q, Oostrom M, et al. Pore-scale supercritical CO_2 dissolution and mass transfer under drainage conditions. *Advances in Water Resources*, 2017, 100: 14-25
26 Zhao B, MacMinn CW, Juanes R. Wettability control on multiphase flow in patterned microfluidics. *Proceedings of the National Academy of Sciences*, 2016, 113(37): 10251-10256
27 Xu W, Ok JT, Xiao F, et al. Effect of pore geometry and interfacial tension on water-oil displacement efficiency in oil-wet microfluidic porous media analogs. *Physics of Fluids*, 2014, 26(10): 093102
28 Zhang C, Oostrom M, Wietsma TW, et al. Influence of viscous and capillary forces on immiscible fluid displacement: Pore-scale experimental study in a water-wet micromodel demonstrating viscous and capillary fingering. *Energy & Fuels*, 2011, 25(8): 3493-3505
29 Cottin C, Bodiguel H, Colin A. Influence of wetting conditions on drainage in porous media: A microfluidic study. *Physical Review E*, 2011, 84(2): 026311
30 Raeesi B, Piri M. The effects of wettability and trapping on relationships between interfacial area, capillary pressure and saturation in porous media: A pore-scale network modeling approach. *Journal of Hydrology*, 2009, 376(3): 337-352
31 Liu H, Ju Y, Wang N, et al. Lattice Boltzmann modeling of con- tact angle and its hysteresis in two-phase flow with large viscosity difference. *Physical Review E*, 2015, 92(3): 033306
32 Bandara U, Tartakovsky AM, Oostrom M, et al. Smoothed particle hydrodynamics pore-scale simulations of unstable immiscible flow in porous media. *Advances in Water Resources*, 2013, 62: 356-369
33 Raeini AQ, Bijeljic B, Blunt MJ. Modelling capillary trapping using finite-volume simulation of two-phase flow directly on micro-CT images. *Advances in Water Resources*, 2015, 83: 102-110
34 Ferrari A, Jimenez-Martinez J, Borgne TL, et al. Challenges in modeling unstable two-phase flow experiments in porous micromodels. *Water Resources Research*, 2015, 51(3): 1381-1400
35 Ferrari A, Lunati I. Direct numerical simulations of interface dynamics to link capillary pressure and total surface energy. *Advances*
space*in Water Resources*, 2013, 57: 19-31

36 Greenshields C. OpenFOAM User Guide. Version 2.4. 0. OpenFOAM Foundation Ltd, 2015

37 Batzle M, Wang Z. Seismic properties of pore fluids. *Geophysics*, 1992, 57(11): 1396-408

38 Wang S, Tokunaga TK. Capillary pressure-saturation relations for supercritical CO_2 and brine in limestone/dolomite sands: Implications for geologic carbon sequestration in carbonate reservoirs. *En- vironmental Science & Technology*, 2015, 49 (13): 7208-7217

39 Abra`moff MD, Magalha˜es PJ, Ram SJ. Image processing with Im- age J. *Biophotonics International*, 2004, 11(8): 36-42

40 Roman S, Soulaine C, AlSaud MA, et al. Particle velocimetry anal- ysis of immiscible two-phase flow in micromodels. *Advances in Water Resources*, 2015, 95: 199-211

41 Horgue P, Augier F, Duru P, et al. Experimental and numerical study of two-phase flows in arrays of cylinders. *Chemical Engineering Science*, 2013, 102(15): 335-345

42 Geistlinger H, Ataei-Dadavi I, Mohammadian S, et al. The impact of pore structure and surface roughness on capillary trapping for 2-D and 3-D porous media: Comparison with percolation theory. *Water Resources Research*, 2015, 51(11): 9094-9111

43 Mohammadian S, Geistlinger H, Vogel HJ. Quantification of gas-phase trapping within the capillary fringe using computed microto- mography. *Vadose Zone Journal*, 2015, 14(5):

44 Jimenez-Mart´ınez J, Porter ML, Hyman JD, et al. Mixing in a three- phase system: Enhanced production of oil-wet reservoirs by CO_2 injection. *Geophysical Research Letter*, 2016, 43(1): 196-205

45 Land CS. Calculation of imbibition relative permeability for two- and three-phase flow from rock properties. *Society of Petroleum En- gineers Journal*, 1968, 8(2): 149-156

46 Jerauld G. General three-phase relative permeability model for Prud- hoe Bay. *SPE Reservoir Engineering*, 1997, 12(04): 255-263

47 Spiteri EJ, Juanes R, Blunt MJ, et al. A new model of trapping and relative permeability hysteresis for all wettability characteristics. *SPE Journal*, 2008, 13(3): 277-288